Acta Pharmacologica Sinica

www.nature.com/aps

ARTICLE

Anemoside B4 inhibits enterovirus 71 propagation in mice through upregulating 14-3-3 expression and type I interferon responses

Nai-xin Kang[1,2], Yue Zou[1], Qing-hua Liang[1], Yan-er Wang[1], Yan-li Liu[1], Guo-qiang Xu[1], Han-dong Fan[3], Qiong-ming Xu[1,2], Shi-lin Yang[1] and Di Yu[4]

Enterovirus 71 (EV71) is the major pathogens of human hand, foot, and mouth disease (HFMD). EV71 efficiently escapes innate immunity responses of the host to cause infection. At present, no effective antiviral drugs for EV71 are available. Anemoside B4 (B4) is a natural saponin isolated from the roots of *Pulsatilla chinensis* (Bunge) Regel. *P. chinensis* extracts that shows a wide variety of biological activities. In this study, we investigated the antiviral activities of B4 against EV71 both in cell culture and in suckling mice. We showed that B4 (12.5–200 μM) dose dependently increased the viability of EV71-infected RD cells with an IC_{50} value of 24.95 ± 0.05 μM against EV71. The antiviral activity of B4 was associated with enhanced interferon (IFN)-β response, since knockdown of IFN-β abolished its antiviral activity. We also confirmed that the enhanced IFN response was mediated via activation of retinoic acid-inducible gene I (RIG-I) like receptors (RLRs) pathway, and it was executed by upregulation of 14-3-3 protein, which disrupted the interaction between yes-associated protein (YAP) and interferon regulatory factor 3 (IRF3). By using amino acids in cell culture (SILAC)-based proteomics profiling, we identified the Hippo pathway as the top-ranking functional cluster in B4-treated EV71-infected cells. In vivo experiments were conducted in suckling mice (2-day-old) infected with EV71 and subsequently B4 ($200\ mg \cdot kg^{-1} \cdot d^{-1}$, i.p.) was administered for 16 days. We showed that B4 administration effectively suppressed EV71 replication and improved muscle inflammation and limb activity. Meanwhile, B4 administration regulated the expressions of HFMD biomarkers IL-10 and IFN-γ, attenuating complications of EV71 infection. Collectively, our results suggest that B4 could enhance the antiviral effect of IFN-β by orchestrating Hippo and RLRs pathway, and B4 would be a potential lead compound for developing an anti-EV71 drug.

Keywords: human hand, foot, and mouth disease; enterovirus 71; anemoside B4; type I IFN; Hippo pathway; 14-3-3 protein

Acta Pharmacologica Sinica (2022) 43:977–991; https://doi.org/10.1038/s41401-021-00733-1

INTRODUCTION

Enterovirus 71 (EV71), a member of the *Picornaviridae* family [1], typically causes human hand, foot, and mouth disease (HFMD) with neurological and systemic complications in young children and infants. Infection with the Enterovirus 71 (EV71) can even lead to severe neurological disease, including fatal encephalitis, aseptic meningitis, or acute flaccid paralysis [2]. According to the surveillance report on HFMD in 2014, the incidence of HFMD in China is 203.16/100,000, while the mortality is 18.03/100,000 [3]. Existed EV71 vaccines are often unsuccessful due to the generation of viral mutants and less effective [4, 5]. Identifying novel antiviral drugs is therefore of critical importance.

Innate immunity serves as the host's first line of defense against pathogen invasion. The retinoic acid-inducible gene I (RIG-I)-like receptors (RLRs) pathway is initiated through the recognition of viral nucleic acid by host pattern recognition receptors. It activates IKK-related kinases that launch transcriptional factors, such as interferon regulatory factor 3 (IRF3), resulting in the expression of type I interferons (IFN-α/IFN-β) [6–9]. IFN-α and IFN-β subsequently activate downstream signaling pathways that induce a diverse set of IFN-stimulated genes and protect host cells against the invading virus [10]. On the other hand, EV71 infection leads RLRs signaling molecules cleavage [11], thus attenuate the type I IFNs production and response. This impaired immunity is also believed to associate with higher morbidity and mortality of the EV71 virus [12].

In addition to this core pathway, other pathways including the Hippo pathway, which is regulated by the nutrient and physical environment of cells, can serve as a potent regulator of IFN production and antiviral defense [13]. Activation of the Hippo pathway triggers phosphorylation and inactivation of the yes-associated protein (YAP) through degradation or cytoplasmic sequestration by 14-3-3 proteins, abrogating the inhibitory effect of YAP/TAZ on TANK-binding kinase 1 (TBK1). Subsequently, unsuppressed TBK1 activates IRF3-mediated expression of type I IFN genes [14]. Therefore, targeted manipulation of the balance

[1]College of Pharmaceutical Science, Soochow University, Suzhou 215123, China; [2]State Key Laboratory of Bioactive Substance and Function of Natural Medicines, Institute of Materia Medica, Chinese Academy of Medical Sciences and Peking Union Medical College, Beijing 100050, China; [3]Institute of Aging Research, School of Medicine, Hangzhou Normal University, Hangzhou 310036, China and [4]Department of Immunology, Genetics and Pathology, Science for Life Laboratory, Uppsala University, Uppsala, Sweden
Correspondence: Qiong-ming Xu (xuqiongming@suda.edu.cn)

Received: 31 August 2020 Accepted: 29 June 2021
Published online: 28 July 2021

between Hippo signaling and IFN responses could have therapeutic potential in the field of antiviral therapy.

Medicinal plants have been used widely throughout history for the treatment of infections as traditional healing remedies due to their broad therapeutic spectrum and minimal side effects. Natural products remain promising antiviral drug sources [15]. Anemoside B4 (B4) is a natural saponin constituent isolated from the roots of *Pulsatilla chinensis* (Bunge) Regel. *P. chinensis* extracts possessed a wide variety of biological activities, such as antitumor [16, 17], immuno-modification, and immunological adjuvant activities [18]. As reported B4 could inhibit the secretion of cytokines in Porcine circoviruses-induced endothelial cells [19] and lipopolysaccharide-induced rat intestinal microvascular endothelial cells [20]. Moreover, our previous research showed that B4 presented anti-inflammatory and immune-modulatory activities in vivo through inhibition of the NF-κB pathway mediated pro-inflammatory response [21].

However, the clear role of B4 on the innate immune response and its ability to inhibit EV71 propagation has not been investigated. In this study, we found that B4 exhibited significant anti-EV71 activities both in vitro and in vivo. It is the first report that B4 significantly inhibited EV71 propagation through upregulating 14-3-3 and activating the type I IFN responses.

MATERIALS AND METHODS

Viruses, drugs, cell lines, and mice

Enterovirus 71 strain SHAPHC695F/SH/CHN/10 (695F) was isolated from a 1.8-year-old patient in Shanghai Public Health Clinical Center in 2010 [22]. Human rhabdomyosarcoma cell line (RD) and African Green Monkey Kidney cell line (Vero) were purchased from ATCC (CCL-136, CCL-81, Manassas, VA, USA). B4 (10.0 g) was isolated in our lab from the roots of *P. chinensis* (No. 09-04-18-01), and the structure was identified by comparison of its spectroscopic data with those of the reported [23]. The purity of B4 was determined as 99.9% by analytical HPLC with PDA detection. Specific-pathogen-free ICR mice (Charles River Laboratories, Wilmington, MA, USA) were maintained in the animal facility of the Shanghai Public Health Clinical Center. Pups of the same experimental group were housed together in an environment of 50% humidity at 22 °C under a 12-h light/dark cycle. They were kept with their mothers to provide food.

Ethics statement

Specific-pathogen-free suckling ICR mice were carried out under the National Institute of Health Guide for the Care and Use of Laboratory Animals and approved by the Shanghai Public Health Clinical Center Laboratory Animal Welfare and Ethics Committee with the number of 2019-A006-01.

EV71 infection and drugs administration in mice

Two-day-old suckling mice (2.0–2.3 g) were injected with 10^6 pfu EV71 (strain 695F) and subsequently underwent intraperitoneal (i.p.) injection with 1–5 μL of B4 to achieve the dosage of 200 mg kg^{-1} of B4 ($n = 10$), or an equivalent volume of physiological saline was injected in the EV71 group ($n = 10$). The drug was injected every day for 16 days. Infected mice were monitored daily for signs of morbidity and mortality. The sickness of mice was evaluated using a graded score (0, healthy; 1, slow movement; 2, weakness in hind limbs; 3, paralysis in single limb; 4, paralysis in two limbs; and 5, death). To better illustrate the recovery of the surviving mice, deaths were calculated into the average score only once at the first observation date. All mouse muscle tissues and serum were obtained from the 5th-day post infection. The tissues were further assayed for quantitative reverse transcriptase-PCR (qRT-PCR), histology, and immunohistochemistry analysis.

Histology and immunohistochemistry analysis

Routine hematoxylin and eosin (H&E) staining of various mouse skeletal muscles was performed using 3.7% formaldehyde-fixed, paraffin-embedded, and sectioned (4 mm thick) tissues. The sections were deparaffinized, washed in phosphate-buffered saline (PBS, 0.01 M, pH 7.2) 5 min for three times, then heated at 100 °C in a microwave oven 2 min for six times, incubated in 3% H_2O_2 in deionized water for 10 min to block endogenous peroxides activity, and then washed 5 min with PBS for three times. The sections were incubated overnight at 4 ˚C with anti-EV71 VP-1 monoclonal antibody (MAB979, Millipore, Billerica, MA, USA) and IFN-β antibody (NBP1-77288, Novus Biologicals, Littleton, CO, USA). After washing 5 min with PBS for three times, the appropriate HRP-polymer anti-mouse/rabbit immunoglobulin G was added to the sections and incubated at 37 °C for 20 min. The sections were then washed 5 min with PBS for three times, and the color was developed with DAB (34065, Thermo Scientific, Waltham, MA, USA) for 3–5 min. The nuclei were lightly counterstained with hematoxylin. Rigorous controls (matched tissue sections negative for EV71) were included in parallel to ensure the signals obtained were specific to viral antigen. The concentration of IL-10 and IFN-γ in serum was detected by U-Plex Biomarker Group 1 (ms) Assays (K15069l-1, Meso Scale Diagnostics, Rockville, MD, USA) with Meso Sector S 600 (Meso Scale Diagnostics, Rockville, MD, USA).

Cell cultures and virus infection

RD and Vero cells were cultured in Dulbecco's Modified Eagle's Medium (DMEM, Life Technologies, Carlsbad, CA, USA) supplemented with 10% fetal bovine serum (FBS, Gibco, Carlsbad, CA, USA) and 1% penicillin/streptomycin (Life Technologies, Carlsbad, CA, USA). RD cells were used for propagation and plaque titration of EV71. The virus infection was performed at a multiplicity of infectivity of 1 in DMEM medium free of FBS. The EV71 virus stocks were collected from the supernatants of infected cells at 24 h post infection (hpi). Cell viability was measured using a cell counting kit (CCK-8; Dojindo Laboratories, Kumamoto, Japan).

Titration assay

The titers of the virus stocks were determined by a TCID50 assay, and the stocks were aliquoted and stored at −80 °C. As of the TCID50 assay, serially diluted viruses from 10^{-1} to 10^{-9} in DMEM were inoculated to RD cells in 96-well plates, and the cells were incubated for seven days at 37 °C. TCID50 were calculated by counting the wells with cytopathic effect in infected RD cells using the formula: $\log_{10} \mathrm{TCID50} = L - d \times (s - 0.5)$, where L is the log of the lowest dilution, d is the difference between dilution steps, and s is the sum of the proportion of positive wells.

Quantitative RT-PCR

Total RNA from infected tissues or cells was isolated using the Trizol reagent (Invitrogen, Carlsbad, CA, USA) according to the manufacturer's instruction. Complementary DNA was generated from 2 μg of the RNA by reverse transcription with oligo-T (dT) primer. qRT-PCR was performed with primers for VP-1, IFN-β, and 14-3-3β (summarized in Table S1 in the Supplementary information) using a CFX96™ real-time system (Bio-Rad, Hercules, CA, USA). The mRNA levels of target genes were normalized to β-Actin or GAPDH levels and were compared by the $2^{-\Delta\Delta Ct}$ method.

ELISA assay for IFN-β

Cell culture supernatants were harvested from uninfected and infected RD cells with or without B4 administration at indicated time points, followed by centrifugation at $1000 \times g$ for 15 min at 4 °C. A human IFN-β ELISA kit (Multisciences, LiankeBio, Shanghai, China) was used following the manufacturer's protocol.

Stable-isotope labeling by amino acids in cell culture (SILAC) based proteomic profiling

DMEM media were made for SILAC experiments by adding light ($^{12}C_6$) or heavy ($^{13}C_6$) lysine and arginine into the DMEM without *L*-lysine and *L*-arginine (Thermo Scientific, Waltham, MA, USA), supplemented with dialyzed FBS (Invitrogen, Carlsbad, CA, USA). RD cells were cultured in these two DMEM media for a week to enable complete labeling.

Cell protein samples were prepared and analyzed as previously described before [24]. In a typical procedure, equal amounts of cell protein samples from light- or heavy-labeled cells were mixed. Then, 100 μg of protein samples were digested by using trypsin, and then the peptide samples were desalted with a C18 solid-phase column, dried in a vacuum centrifugal concentrator, and dissolved in 0.1% formic acid for MS/MS analysis. LC–MS/MS analysis was conducted using Orbitrap mass spectrometer (Thermo Scientific, Waltham, MA, USA). Raw MS data were matched by MaxQuant software (version 1.6.1.1) against a human protein database released from UniProt in July, 2017. The SILAC analysis was performed with three biological replicates.

Immunoprecipitation and Immunoblotting analysis

Cells were lysed with 80 μL of RIPA (containing 1% PMSF) (Sigma-Aldrich, St Louis, MO, USA) on ice for 10 min. Cell lysates were centrifuged at 12,000 × *g* for 10 min, then the concentrations was quantified with the bicinchoninic acid assay BCA (Pierce, Rockford, IL, USA). An equal amount of proteins was used for immunoprecipitation and immunoblotting analysis. For Flag-tag protein immunoprecipitation, anti-Flag M2 affinity gel (Sigma-Aldrich, St Louis, MO, USA) was used and the performance followed the technical procedure. Proteins in the lysates were separated by 8%–10% SDS-polyacrylamide gel electrophoresis (SDS-PAGE). The separated proteins were transferred to PVDF membranes (Millipore, Billerica, MA, USA) and probed with the anti-EV71 VP-1 (MAB979, Millipore, Billerica, MA, USA), anti-EV71 3Cpro (GTX630191, GnenTex, Irvine, CA, USA), anti-IRF3 (D614C, Cell Signaling, Danvers, MA, USA), anti-phospho-IRF3 (Ser396, Cell Signaling, Danvers, MA, USA), anti-IFN-β (EPR12687, Abcam, Waltham, MA, USA), anti-MxA (EPR19967, Abcam, Waltham, MA, USA), anti-FLAG (F3165, Millipore, Billerica, MA, USA), anti-YAP (14074, Cell Signaling, Danvers, MA, USA), anti-14-3-3β (sc-25276, Santa Cruz, Dallas, TX, USA), and anti-β-Actin (Sigma-Aldrich, St Louis, MO, USA) primary antibodies overnight at 4 °C. After incubation with an HRP-conjugated secondary antibody (Cell Signaling, Danvers, MA, USA), the specific proteins were visualized using a chemiluminescent HRP substrate (Millipore, Billerica, MA, USA).

Confocal immunofluorescence

The target cells were fixed with paraformaldehyde for 30 min, washed three times with PBS, permeabilized with 0.2% Triton X-100 buffer, and blocked with PBS containing 1% bovine serum albumin (BSA) for 1 h at room temperature. Then, the cells were incubated with the primary antibody overnight at 4 °C and washed three times with PBS containing 0.01% Tween 20 and 1% BSA. Then, cells were incubated with their respective secondary antibodies for another 1 h. The cells were then washed and stained with DAPI (4083S, Cell Signaling, Danvers, MA, USA) to detect nuclei. Images were captured with confocal laser microscopy (LSM 710, Carl Zeiss, Germany).

Cell transfection

The siRNA targeting human IFN-β, 14-3-3β, or control siRNA with scrambled sequence were purchased from Ribobio (RiboBio, Guangzhou, China). To knockdown IFN-β or 14-3-3β expression, cells were transfected with the respective siRNAs using Lipofectamine 3000 (L3000-015, Invitrogen, Carlsbad, CA, USA). Twenty-four hours after transfection, the medium was changed using DMEM supplemented with B4 or DMEM for 1 h. Cells were harvested for future study after they had been infected with EV71 for 24 h.

Statistical analysis

Comparison of survival was performed with Mantel–Cox test. The 50% inhibitory concentration (IC_{50}) were calculated by software (GraphPad Software, La Jolla, CA, USA). All data were expressed as means ± SEM. The two-tailed Student's *t*-test was used to evaluate these data. Differences with $P < 0.05$ were considered statistically significant.

RESULTS

B4 exhibited antiviral activity against EV71 in RD cells

To address whether B4 exhibit antiviral activity, we incubated RD cells with different concentrations (12.5–200 μM) of B4 prior to infection with EV71. B4 exhibit strong antiviral effect in a dose-dependent manner, evidenced as both the cell viability reached 100% (Fig. 1a) and the cell morphology remained unchanged (Fig. 1b) in EV71-infected cell at B4 dosage of 200 μM. The IC_{50} of B4 against EV71 was calculated as 24.95 ± 0.05 μM after linear regression in RD cells (Fig. 1c). Importantly, B4 itself did not show any toxicity to RD cells in the tested concentrations (Fig. 1d).

We also quantified the progeny virus titer in the supernatants after EV71 infection with and without B4 treatment. A clear inhibition of virus replication was observed as there is approximately 2-log lower of progeny virus in the supernatant harvested in B4-treated cells compared to untreated cells (Fig. 1e). Next, the antiviral effects were validated by measuring the intracellular viral genomic RNA copies and viral protein levels. B4, at concentration of 200 μM suppressed EV71-induced VP-1 mRNA transcripts in RD cells by ~50% at 24 hpi (Fig. 1f). Consistently, the levels of intracellular VP-1 and main EV71 protease 3Cpro were significantly inhibited by B4 in a dose-dependent manner (Fig. 1g). Taken together, all these data suggested that B4 exhibited strong antiviral effect in vitro by inhibiting viral replication.

Induction of IFN-β is required for B4 to exert its antiviral effects

The potential antiviral mechanisms of B4 against EV71 infection were investigated using a time-of-addition assay. B4 (200 μM) was supplemented to EV71-infected RD cells according to different protocols described (Fig. 2a). When comparing B4 treatment prior, in the meantime, or post EV71 infection, we observed pre-treatment (1 h incubation) of the cells with B4 gives the best antiviral activity (Fig. 2b). This led us to further investigate whether the antiviral effect of B4 was associated with activation of cellular defense pathway. Indeed, we observed B4 sensitizes the cellular defense response during EV71 infection as shown by significantly upregulated levels of IFN-β and IFN-stimulated genes (MxA) (Fig. 2c), whereas compared to cells that were infected by EV71 alone. The virus infection was confirmed by the expression of VP-1 (Fig. 2c). Moreover, the upregulated expression of IFN-β in cell supernatant of B4-treated cells was confirmed by ELISA (Fig. 2d). These results indicated that B4 not only enhanced the virus-triggered IFN-β induction but also IFN-β response.

Critical steps for signal transduction via IFN-β are TBK1-IKKε-induced phosphorylation of IRF3 at Ser396 and subsequent entry of IRF3 into the nucleus [25]. We therefore assessed the effect of B4 on those molecular events. The phosphorylation of IRF3 was significantly decreased after infection with EV71 24 h, however, EV71-induced phosphorylation of IRF3 was dramatically reversed in B4 stimulated cells (Fig. 2e). Moreover, B4 enhanced translocation of p-IRF3 to the nucleus (Fig. 2f, g), compared to cells only infected with EV71 which showed neglectful staining of nuclear p-IRF3, thus confirming the above results.

Further investigations were performed to determine whether IFN-β were required for the antiviral effect of B4. Three specific siRNAs for IFN-β (si-IFN-β No. 1#−3#) were designed, and si-IFN-β

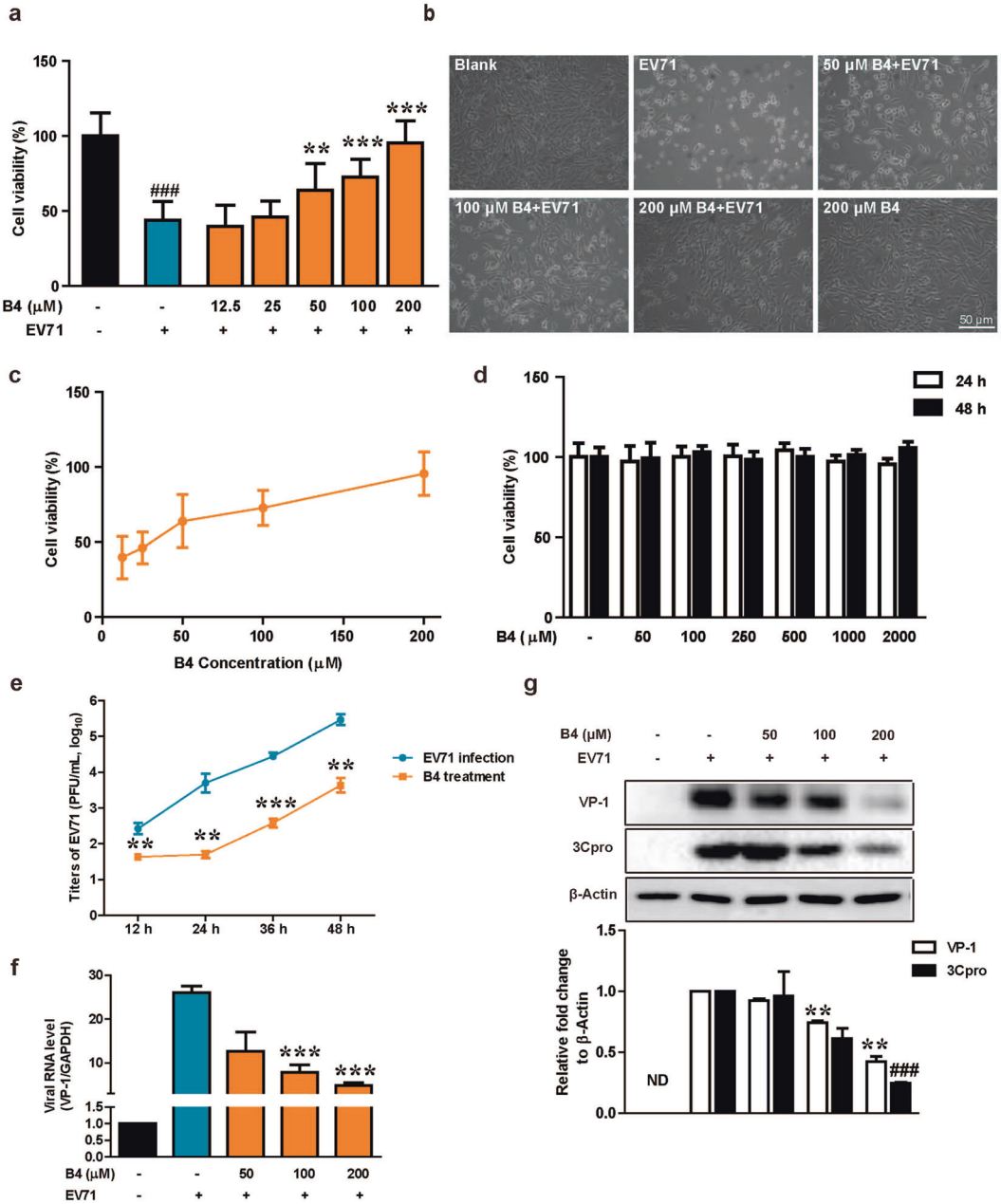

Fig. 1 B4 inhibited EV71 propagation without obvious cytotoxicity. a The anti-EV71 activity of B4 was evaluated by cell viability assays. RD cells were infected with EV71 after treatment with B4 at various concentrations. The viability of the control group (blank cells) was set as 100%; **b** The morphological change of cytopathy effects in RD cells infected with EV71 after treatment with B4 at different concentrations. Scale bar = 50 μm; **c** Dose-response influence of B4 on cytopathic effects induced by EV71, and IC_{50} value was calculated as described in the "Materials and methods"; **d** Evaluation of the cytotoxicity of B4. RD cells were treated with B4 at various concentrations as indicated. The effects of B4 on cell viability were evaluated by cell viability assay at 24 or 48 h. The viability of blank cells was set as 100%; **e** RD cells were treated with different concentrations of B4 before EV71 infection. Cell supernatants were harvested at the 12–48 h post infection and the viral titers were determined by TCID50 assays; **f** Total RNAs of RD cells were prepared from different groups and subjected to qRT-PCR for the VP-1 region of EV71 viral RNA. GAPDH was also analyzed as internal control. Values were expressed as a percentage of RD cells without infection; **g** RD cells were treated with different concentrations of B4 at 24 h before EV71 infection, and then total cell extracts were subjected to Western blot analysis with anti-VP-1 antibody and anti-3Cpro antibody. β-Actin was also analyzed as loading control. Values were expressed as a percentage of RD cells without treatment. Data are presented as mean ± SD ($n = 3$). $^{**}P < 0.01$, $^{***}P < 0.001$ vs cells infected EV71 without treatment and $^{###}P < 0.001$ vs cells without infection.

3# effectively knocked down endogenous IFN-β expression (Fig. 3a). The results from the viability protection assay indicated that IFN-β knockdown suppressed the antiviral effects of B4, decreased viability of infected cells (Fig. 3b). Meanwhile, there were no differences observed in the expression of viral proteins VP-1 and 3Cpro (Fig. 3c) and viral titers (Fig. 3d) in the infected IFN-β knockdown cells, regardless of B4 treatment or not. In addition, we used Vero cells, which lack functional type I IFN genes [26], to confirm the vital role of IFN-β on the antiviral activity of B4. EV71 replication was not affected in Vero cells (Fig. 3e–g), excepting for the improvement of B4-treated cell viability (Fig. 3e, $P < 0.05$, compared with EV71-infected cells). These results

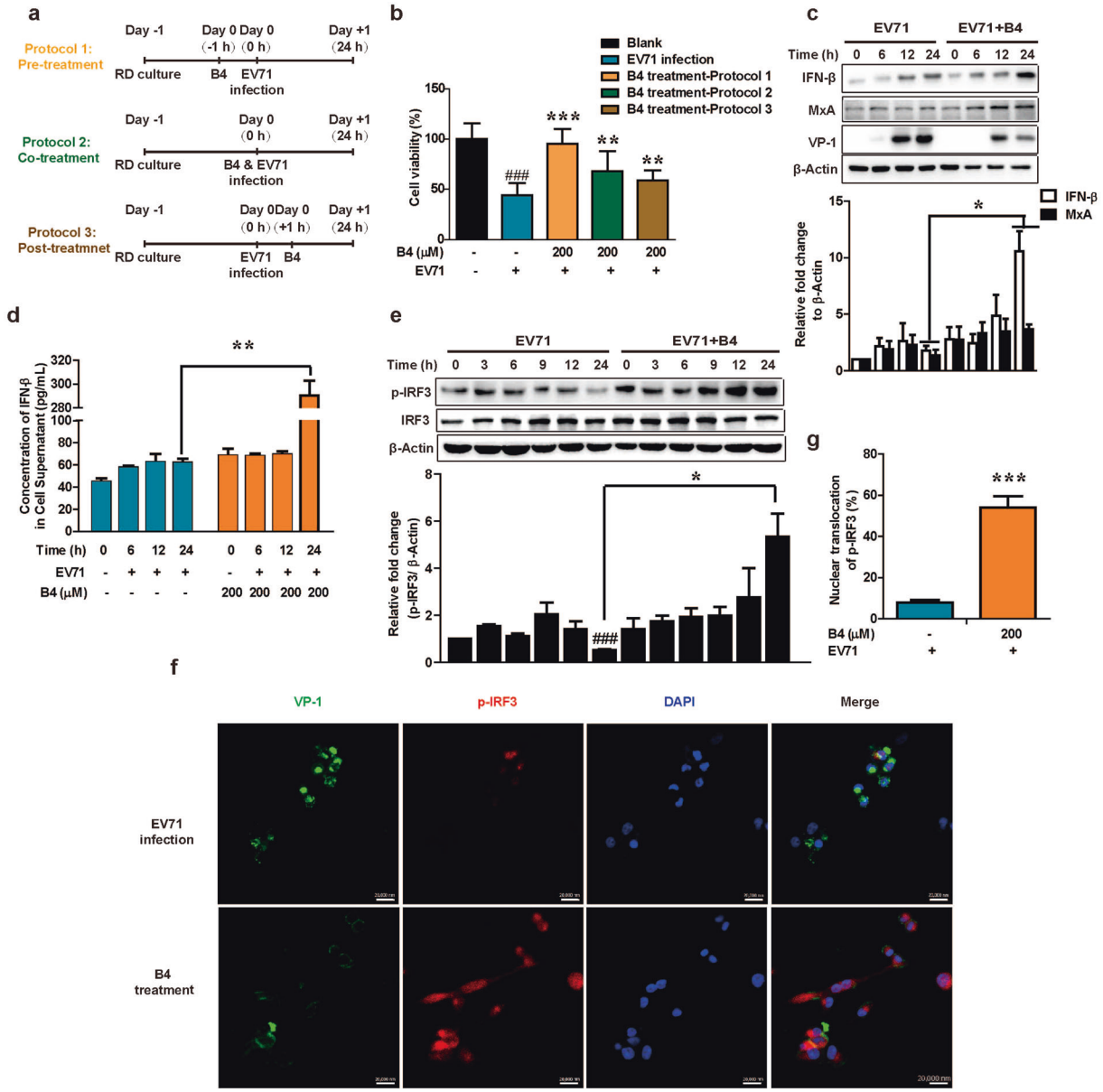

Fig. 2 B4 potentiated virus-triggered RLRs pathway activation. a B4 treatment (200 μM) was performed before or after EV71 infection as indicated in the figure; **b** The viability of RD cells according to different protocols was detected using cell viability assays. The viability of the control group was set as 100%; **c** Total protein of RD cells with or without B4 treatment after infection in different times was subjected to Western blot for detection of IFN-β, MxA, VP-1 levels. β-Actin was also analyzed as loading control; **d** The level of IFN-β in cell supernatants harvested from RD cells with or without B4 administration at different infection time; **e** Total protein of RD cells with or without B4 administration after infection at different times were subjected to Western blot for detection of p-IRF3, IRF3 levels. β-Actin was also analyzed as loading control; **f** Representative confocal microscope image showing localization of p-IRF3 and VP-1. At 24 h after treatment with B4, RD cells were immune-stained with antibodies against p-IRF3 (red), VP-1 (green), and nucleus was stained with DAPI (blue), Scale bar = 20 μm; **g** Quantitation of p-IRF3 nuclear translocation. A total of 400 p-IRF3-positive cells from different fields were counted. Data are presented as mean ± SD ($n = 3$). $^{*}P < 0.05$, $^{**}P < 0.01$ and $^{***}P < 0.001$ vs cells infected EV71 without treatment and $^{\#\#\#}P < 0.001$ vs cells without infection.

indicated that B4 exerted its antiviral function through potentiating the RLRs pathway.

Target profiling of B4 by SILAC-based proteomics analysis

We further investigated the molecular mechanism through which B4 augmented type I IFN production. To identify these regulated proteins, we performed SILAC experiments with or without B4 treatment in EV71-infected cells (Fig. 4a). Briefly, proteomes were lysed from the "light" and "heavy" infected cells incubated with PBS or B4, respectively, and light and heavy proteomes were mixed and finally subjected to trypsin digestion. The digested peptides were analyzed by liquid chromatography tandem mass spectrometry to identify proteins that are affected by B4 administration. After applying a cut-off of 1.4 for the averaged SILAC ratio in the experiment, we collectively identified 92 proteins regulated by B4 (Fig. 4b, $P < 0.05$ and Table 1).

Further, KEGG analysis (Kyoto Encyclopedia of Genes and Genomes of the pathways) associated with these 92 proteins revealed a top-ranking functional cluster of the "Hippo pathway", which includes six proteins (Fig. 4c and Table 2). Among these proteins, 14-3-3 was reported as the molecular scaffolds

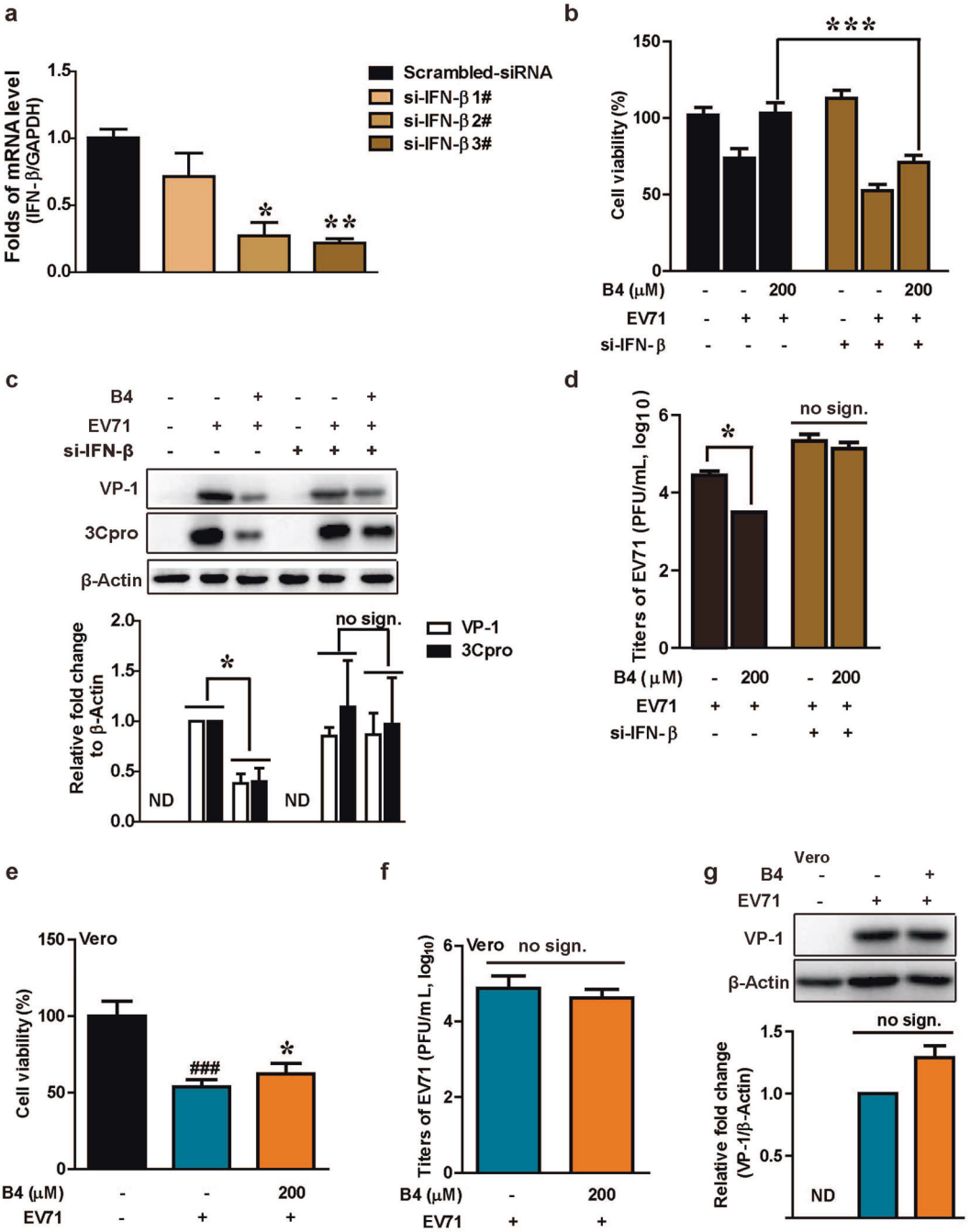

Fig. 3 The inhibitory effect of B4 on EV71 propagation required IFN-β. a RD cells were transfected with si-IFN-β or scrambled-siRNA for 48 h, and IFN-β mRNA levels were determined by qRT-PCR. GAPDH was also analyzed as internal control; RD cells were transfected with IFN-β-specific siRNA and control siRNA for 48 h and then infected with EV71 after B4 treatment. **b** Antiviral activity was determined by the cell viability assay. Cell viability of transfected scrambled-siRNA cells was set 100%. Data are presented as mean ± SD ($n = 3$). ***$P < 0.001$; **c** The levels of VP-1 and 3Cpro were evaluated by immunoblotting with VP-1 and 3Cpro antibodies. β-Actin was also analyzed as loading control. Data are presented as mean ± SD ($n = 3$). *$P < 0.05$, no sign., no significant difference; **d** Cell supernatants were harvested at the 24 h post infection and the viral titers were determined by TCID50 assays. Data are presented as mean ± SD ($n = 3$). *$P < 0.05$, no sign., no significant difference; **e** Vero cells were infected with EV71 after B4 treatment for 24 h. Antiviral activity was determined by the cell viability assay. Cell viability of blank cells was set as 100%; **f** EV71 production in the supernatants was estimated by TCID50 assays; **g** Total cell extracts were subjected to Western blot analysis with anti-VP-1 antibody. β-Actin was also analyzed as a loading control. Data are presented as mean ± SD ($n = 3$). ###$P < 0.001$ vs cells without infection and *$P < 0.05$ vs cells infected EV71 without treatment. no sign., no significant difference.

which exerts an important regulatory function in the IFN response by modulating YAP cellular localization [13]. Immunoblotting analysis confirmed that a twofold increase of 14-3-3β protein level in B4-treated cells compared with that of the PBS-treated cells (Fig. 4d). B4 treatment could also increase 14-3-3β mRNA level (Fig. 4e). Since 14-3-3 protein family members have been implicated in innate immunity, where they function to sequestration of YAP in the cytoplasm. The enhanced 14-3-3β cytoplasm localization in B4-treated cells (Fig. 4f) suggested that 14-3-3β might affect the intracellular localization of YAP.

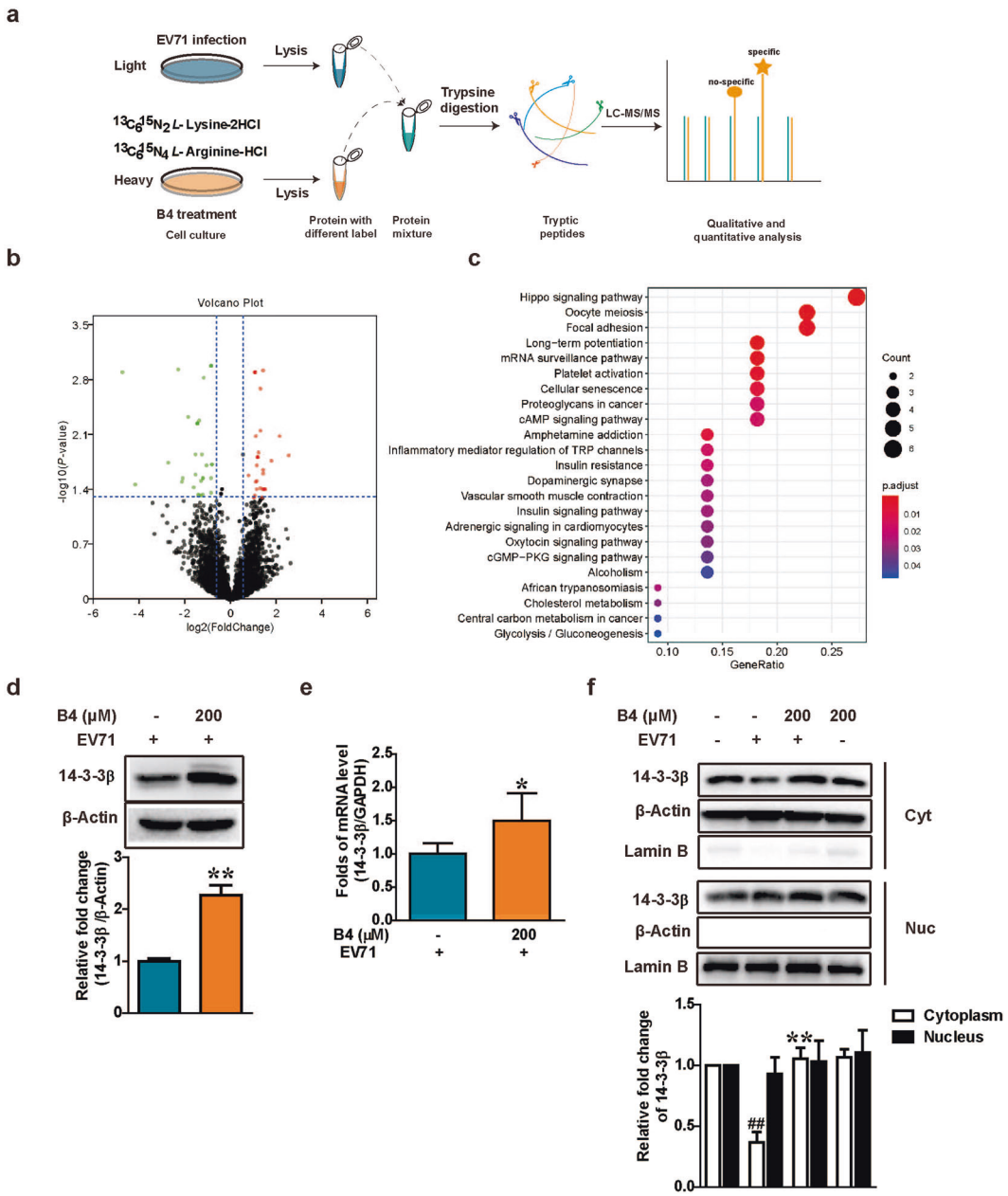

Fig. 4 SILAC-based proteome profiling of the identified proteins in the EV71-infected cells upon B4 administration. a Schedule of SILAC-based proteome profiling; **b** The volcano plot for the MS identified proteins in RD cells. Each data point indicates the $\log2^{\text{fold change}}$ (*X*-axis) with their corresponding $-\log10^{P\ \text{value}}$ (*Y*-axis). The threshold for differential expression (cut-off = fold change >1.4 or <0.7 and $P < 0.05$) is indicated by dashed black lines. Solid green and red respectively depicted the significantly decreased and increased proteins after B4 supplementation; **c** Classification landscape of 92 B4-regulated proteins according to the biological process by KEGG analysis. The number of differentially expressed proteins in each category has been shown. Significantly enriched metabolic or signal transduction pathways in differentially expressed proteins were identified in the Kyoto Encyclopedia of Genes and Genomes (KEGG) database (http://www.genome.jp/kegg); **d** Western blot validation of the expression levels of 14-3-3β in EV71-infected RD cells treated with/without B4. β-Actin was also analyzed as loading control; **e** qRT-PCR validation of the expression levels of 14-3-3β in EV71-infected RD cells treated with/without B4. GAPDH was also analyzed as internal control; **f** Western blot analysis of 14-3-3β in the nuclear and cytoplasm fractions derived from RD cells in different groups. Densitometry analysis 14-3-3β in nuclear and cytoplasm presented relative to the respective controls for the nuclear fraction (laminin B) and the cytoplasmic fraction (β-Actin). Data are presented as mean ± SD ($n = 3$). $^{\#\#}P < 0.01$ vs cells without infection and $^{*}P < 0.05$, $^{**}P < 0.01$ vs cells infected EV71 without treatment.

B4 increases 14-3-3β to interact with YAP and affects its capacity to enhance the RLRs pathway activation

It is reported that YAP participates in negative regulation of type I IFN response, so B4 may enhance type I IFN response by promoting the cytoplasmic sequestration of YAP. Intriguingly, confocal immunofluorescence detected endogenous expression of YAP (immunostaining green) with colocalization of 14-3-3β (immunostaining red) to the cytoplasm after stimulation with B4 administration (Fig. 5a). Meanwhile, we detected the interaction of 14-3-3β, YAP, and IRF3 in FLAG-YAP transfected cells. We found that B4 promoted the association of YAP with 14-3-3β (Fig. 5b).

Table 1. List of proteins that were differentially expressed in the EV71-infected and B4-treated RD cells.

Protein IDs	Protein names	Difference	*P* value
D9ZGG2	Vitronectin OS = Homo sapiens GN = VTN PE = 4 SV = 1	0.036290692	0.001213
ENSEMBL	(Bos taurus) 63 kDa protein	0.053056798	0.033104
A0A024R3E3	Apolipoprotein A-I, isoform CRA_a OS = Homo sapiens GN = APOA1 PE = 3 SV = 1	0.147237674	0.017587
Q9BVT2	Uncharacterized protein (Fragment) OS = Homo sapiens PE = 2 SV = 1	0.196913066	0.001144
F8W696	Apolipoprotein A-I OS = Homo sapiens GN = APOA1 PE = 1 SV = 1	0.222821479	0.031196
Q9Y623	Myosin-4 OS = Homo sapiens GN = MYH4 PE = 2 SV = 2	0.223794357	0.027548
Q5BJD5-3	Isoform 3 of Transmembrane protein 41B OS = Homo sapiens GN = TMEM41B	0.2683121	0.004591
E9PLA9	Caprin-1 (Fragment) OS = Homo sapiens GN = CAPRIN1 PE = 1 SV = 1	0.312360234	0.036091
M0QXM4	Amino acid transporter OS = Homo sapiens GN = SLC1A5 PE = 1 SV = 1	0.330869248	0.025132
Q13501-2	Isoform 2 of Sequestosome-1 OS = Homo sapiens GN = SQSTM1	0.337187171	0.013838
A0A0J9YXB3	Ras-related protein Rap-1b-like protein OS = Homo sapiens PE = 4 SV = 1	0.358030279	0.005495
A0A024RB87	RAP1B, member of RAS oncogene family, isoform CRA_a OS = Homo sapiens GN = RAP1B PE = 4 SV = 1	0.358030279	0.005495
P61224-4	Isoform 4 of Ras-related protein Rap-1b OS = Homo sapiens GN = RAP1B	0.358030279	0.005495
B7ZB78	Ras-related protein Rap-1b OS = Homo sapiens GN = RAP1B PE = 1 SV = 1	0.358030279	0.005495
F5GZG1	Ras-related protein Rap-1b (Fragment) OS = Homo sapiens GN = RAP1B PE = 1 SV = 8	0.358030279	0.005495
A6NIZ1	Ras-related protein Rap-1b-like protein OS = Homo sapiens PE = 2 SV = 1	0.358030279	0.005495
P61224-3	Isoform 3 of Ras-related protein Rap-1b OS = Homo sapiens GN = RAP1B	0.358030279	0.005495
F5H823	Ras-related protein Rap-1b (Fragment) OS = Homo sapiens GN = RAP1B PE = 1 SV = 1	0.358030279	0.005495
Q5JR06	Rho-related GTP-binding protein RhoC (Fragment) OS = Homo sapiens GN = RHOC PE = 4 SV = 8	0.360103978	0.044545
E9M4D4	Hemoglobin alpha-1 globin chain (Fragment) OS = Homo sapiens GN = HBA1 PE = 3 SV = 1	0.369676242	0.005119
Q14314	Fibroleukin OS = Homo sapiens GN = FGL2 PE = 1 SV = 1	0.376610684	0.046317
C9JEV9	Cleavage and polyadenylation-specificity factor subunit 4 OS = Homo sapiens GN = CPSF4 PE = 1 SV = 1	0.389862932	0.045542
Q9BZZ5-2	Isoform 2 of Apoptosis inhibitor 5 OS = Homo sapiens GN = API5	0.392773364	0.029979
E9PN67	Ninein OS = Homo sapiens GN = NIN PE = 1 SV = 1	0.405214123	0.013897
D3DWY4	HCG17955, isoform CRA_a OS = Homo sapiens GN = hCG_17955 PE = 4 SV = 1	0.413756627	0.045437
B1APM4	Sterol O-acyltransferase 1 (Fragment) OS = Homo sapiens GN = SOAT1 PE = 1 SV = 1	0.415248472	0.028046
Q3B790	High-mobility group nucleosome binding domain 1 OS = Homo sapiens GN = HMGN1 PE = 2 SV = 1	0.422996566	0.027411
E3WH17	Tyrosine-protein kinase receptor OS = Homo sapiens GN = SQSTM1-ALK PE = 2 SV = 1	0.431998659	0.001435
P05114	Non-histone chromosomal protein HMG-14 OS = Homo sapiens GN = HMGN1 PE = 1 SV = 3	0.471847526	0.018896
Q68D08	Uncharacterized protein DKFZp686B04128 OS = Homo sapiens GN = DKFZp686B04128 PE = 2 SV = 1	0.534163081	0.042845
P30044-4	Isoform 4 of Peroxiredoxin-5, mitochondrial OS = Homo sapiens GN = PRDX5	0.536668425	0.027336
Q9H0U4	Ras-related protein Rab-1B OS = Homo sapiens GN = RAB1B PE = 1 SV = 1	0.537732569	0.001021
Q6FIG4	RAB1B protein OS = Homo sapiens GN = RAB1B PE = 2 SV = 1	0.537732569	0.001021
E9PLD0	Ras-related protein Rab-1B OS = Homo sapiens GN = RAB1B PE = 1 SV = 1	0.537732569	0.001021
M0QYL7	Heterogeneous nuclear ribonucleoprotein L (Fragment) OS = Homo sapiens GN = HNRNPL PE = 1 SV = 1	0.55807707	0.018602
M0R1W6	Heterogeneous nuclear ribonucleoprotein L (Fragment) OS = Homo sapiens GN = HNRNPL PE = 1 SV = 1	0.55807707	0.018602
P20340-4	Isoform 4 of Ras-related protein Rab-6A OS = Homo sapiens GN = RAB6A	0.718364068	0.043555
Q6FGX3	RAB6A protein OS = Homo sapiens GN = RAB6A PE = 2 SV = 1	0.718364068	0.043555
P20340-2	Isoform 2 of Ras-related protein Rab-6A OS = Homo sapiens GN = RAB6A	0.718364068	0.043555
Q53ET8	RAB6A, member RAS oncogene family isoform a variant (Fragment) OS = Homo sapiens PE = 2 SV = 1	0.718364068	0.043555
A0A024R5J5	H.sapiens ras-related Hrab6 protein OS = Homo sapiens GN = RAB6A PE = 2 SV = 1	0.718364068	0.043555
Q53S08	Rab6C OS = Homo sapiens GN = RAB6C PE = 2 SV = 1	0.718364068	0.043555
P62136	Serine/threonine-protein phosphatase PP1-alpha catalytic subunit OS = Homo sapiens GN = PPP1CA PE = 1 SV = 1	0.743715738	0.038147
Q9UPN1	Serine/threonine-protein phosphatase (Fragment) OS = Homo sapiens GN = PPP1CC PE = 3 SV = 1	0.743715738	0.038147
A0A087WYY5	Serine/threonine-protein phosphatase OS = Homo sapiens GN = PPP1CC PE = 1 SV = 1	0.743715738	0.038147
A0A140VJS9	Serine/threonine-protein phosphatase OS = Homo sapiens PE = 2 SV = 1	0.743715738	0.038147
P36873	Serine/threonine-protein phosphatase PP1-gamma catalytic subunit OS = Homo sapiens GN = PPP1CC PE = 1 SV = 1	0.743715738	0.038147
E9PMD7	Serine/threonine-protein phosphatase (Fragment) OS = Homo sapiens GN = PPP1CA PE = 1 SV = 1	0.743715738	0.038147
B3KXM2	Serine/threonine-protein phosphatase OS = Homo sapiens PE = 2 SV = 1	0.743715738	0.038147
P36873-2	Isoform Gamma-2 of Serine/threonine-protein phosphatase PP1-gamma catalytic subunit OS = Homo sapiens GN = PPP1CC	0.743715738	0.038147
F8VR82	Serine/threonine-protein phosphatase OS = Homo sapiens GN = PPP1CC PE = 1 SV = 1	0.743715738	0.038147

Table 1. continued

Protein IDs	Protein names	Difference	*P* value
E7ETD8	Serine/threonine-protein phosphatase (Fragment) OS = Homo sapiens GN = PPP1CB PE = 1 SV = 1	0.743715738	0.038147
F8W0W8	Serine/threonine-protein phosphatase OS = Homo sapiens GN = PPP1CC PE = 1 SV = 1	0.743715738	0.038147
F8VYE8	Serine/threonine-protein phosphatase OS = Homo sapiens GN = PPP1CC PE = 1 SV = 1	0.743715738	0.038147
B4E163	Serine/threonine-protein phosphatase OS = Homo sapiens PE = 2 SV = 1	0.743715738	0.038147
B4DJ75	Serine/threonine-protein phosphatase OS = Homo sapiens PE = 2 SV = 1	0.743715738	0.038147
B7ZB67	Serine/threonine-protein phosphatase OS = Homo sapiens PE = 2 SV = 1	0.743715738	0.038147
P62136-3	Isoform 3 of Serine/threonine-protein phosphatase PP1-alpha catalytic subunit OS = Homo sapiens GN = PPP1CA	0.743715738	0.038147
A0A075B6E2	40 S ribosomal protein S19 OS = Homo sapiens GN = RPS19 PE = 1 SV = 1	1.40717057	0.013806
A0PK02	PLXNB2 protein OS = Homo sapiens GN = PLXNB2 PE = 2 SV = 1	1.665784305	0.025289
P31946-2	Isoform Short of 14-3-3 protein beta/alpha OS = Homo sapiens GN = YWHAB	1.976592808	0.048085
V9HWD6	Epididymis secretory protein Li 1 OS = Homo sapiens GN = HEL-S-1 PE = 2 SV = 1	1.976592808	0.048085
E7EPK1	Septin-7 OS = Homo sapiens GN = SEPT7 PE = 1 SV = 2	2.008020754	0.046584
Q59EQ2	Tyrosine 3-monooxygenase/tryptophan 5-monooxygenase activation protein, beta polypeptide variant (Fragment) OS = Homo sapiens PE = 2 SV = 1	2.021518423	0.00124
Q4VY20	14-3-3 protein beta/alpha (Fragment) OS = Homo sapiens GN = YWHAB PE = 1 SV = 1	2.021518423	0.00124
A0A0J9YWE8	14-3-3 protein beta/alpha OS = Homo sapiens GN = YWHAB PE = 1 SV = 1	2.021518423	0.00124
Q4VY19	14-3-3 protein beta/alpha (Fragment) OS = Homo sapiens GN = YWHAB PE = 1 SV = 1	2.021518423	0.00124
A0A0J9YWZ2	14-3-3 protein beta/alpha (Fragment) OS = Homo sapiens GN = YWHAB PE = 1 SV = 1	2.021518423	0.00124
V9HW12	Epididymis secretory sperm binding protein Li 2a OS = Homo sapiens GN = HEL-S-2a PE = 2 SV = 1	2.062785502	0.008012
Q3LIE9	Predicted protein product of Nbla02942 OS = Homo sapiens GN = Nbla02942 PE = 2 SV = 1	2.08257625	0.030758
Q2F831	Tyrosine 3-monooxygenase/tryptophan 5-monooxygenase activation protein zeta (Fragment) OS = Homo sapiens PE = 2 SV = 1	2.121902404	0.030231
P63104	14-3-3 protein zeta/delta OS = Homo sapiens GN = YWHAZ PE = 1 SV = 1	2.155853586	0.019147
E7EX29	14-3-3 protein zeta/delta (Fragment) OS = Homo sapiens GN = YWHAZ PE = 1 SV = 1	2.168367928	0.037808
B7Z2E6	14-3-3 protein zeta/delta OS = Homo sapiens GN = YWHAZ PE = 1 SV = 1	2.181838368	0.01475
B0AZS6	14-3-3 protein zeta/delta OS = Homo sapiens GN = YWHAZ PE = 1 SV = 1	2.181838368	0.01475
P63104-2	Isoform 2 of 14-3-3 protein zeta/delta OS = Homo sapiens GN = YWHAZ	2.181838368	0.01475
H0YB80	14-3-3 protein zeta/delta (Fragment) OS = Homo sapiens GN = YWHAZ PE = 1 SV = 1	2.181838368	0.01475
P09960-3	Isoform 3 of Leukotriene A-4 hydrolase OS = Homo sapiens GN = LTA4H	2.275612857	0.012909
O14737	Programmed cell death protein 5 OS = Homo sapiens GN = PDCD5 PE = 1 SV = 3	2.392694947	0.006909
Q5BKZ1-3	Isoform 3 of DBIRD complex subunit ZNF326 OS = Homo sapiens GN = ZNF326	2.415639198	0.002005
H3BUH7	Fructose-bisphosphate aldolase A (Fragment) OS = Homo sapiens GN = ALDOA PE = 1 SV = 1	2.416603874	0.036982
A0A1B0GUI2	Zinc finger CCCH-type-containing 11B pseudogene OS = Homo sapiens GN = ZC3H11B PE = 1 SV = 1	2.529644374	0.049237
Q3HM38	Programmed cell death 5 short isoform OS = Homo sapiens GN = PDCD5 PE = 1 SV = 1	2.584453167	0.021526
P00338-5	Isoform 5 of *L*-lactate dehydrogenase A chain OS = Homo sapiens GN = LDHA	2.604389461	0.038122
P00338-2	Isoform 2 of *L*-lactate dehydrogenase A chain OS = Homo sapiens GN = LDHA	2.604389461	0.038122
Q8TC62	Septin-7 OS = Homo sapiens GN = SEPT7 PE = 2 SV = 3	2.612097531	0.001164
F5GXY2	*L*-lactate dehydrogenase A chain (Fragment) OS = Homo sapiens GN = LDHA PE = 1 SV = 8	2.63163118	0.02428
F5GYU2	*L*-lactate dehydrogenase A chain (Fragment) OS = Homo sapiens GN = LDHA PE = 1 SV = 1	2.72593762	0.037778
F5GXH2	*L*-lactate dehydrogenase A chain (Fragment) OS = Homo sapiens GN = LDHA PE = 1 SV = 1	2.72593762	0.037778
A2VCM6	PTMS protein (Fragment) OS = Homo sapiens GN = PTMS PE = 2 SV = 1	3.375796745	0.016522
Q8NI35	InaD-like protein OS = Homo sapiens GN = PATJ PE = 1 SV = 3	4.260228873	0.008159
A0A0A0MSA4	Band 4.1-like protein 3 OS = Homo sapiens GN = EPB41L3 PE = 1 SV = 1	5.637035391	0.014217

We then tested whether the knockdown of 14-3-3 affects B4's capacity to inhibit EV71 propagation and the RLRs pathway activation. The influence of 14-3-3 on B4-enhanced RLRs pathway activation and antiviral efficacy was analyzed by siRNA knockdown of 14-3-3β. Gene-silencing efficacy was examined by qRT-PCR and Western blot, and si-14-3-3β 1# effectively knocked down endogenous 14-3-3β expression (Fig. 5c, d). 14-3-3β knockdown dramatically inhibited the viability of the infected cells upon B4 stimulation (Fig. 5e). Moreover, the interaction of 14-3-3β and YAP in B4-treated cells was disturbed by 14-3-3β knockdown (Fig. 5f). Meanwhile, knockdown of 14-3-3β increased the association of YAP with IRF3 (Fig. 5f). Consistent with these results, B4-induced IFN-β expression and IFN-β response (MxA expression) were also decreased by 14-3-3β knockdown, and the downregulated antiviral activity was confirmed by the expression of VP-1 (Fig. 5g). These results suggested that 14-3-3 was required for full activation of RLRs signaling and antiviral efficacy of B4.

Table 2. KEGG analysis of differentially expressed proteins in the EV71-infected and B4-treated RD cells.

ID	Description	*P* value	Gene ID	Count
hsa04390	Hippo signaling pathway	2.98×10^{-6}	5499/5501/5500/7529/7534/10207	6
hsa04114	Oocyte meiosis	2.01×10^{-5}	5499/5501/5500/7529/7534	5
hsa04510	Focal adhesion	0.000185	7448/5908/5499/5501/5500	5
hsa04720	Long-term potentiation	3.16×10^{-5}	5908/5499/5501/5500	4
hsa03015	mRNA surveillance pathway	0.000106	10898/5499/5501/5500	4
hsa04611	Platelet activation	0.000349	5908/5499/5501/5500	4
hsa04218	Cellular senescence	0.000914	8878/5499/5501/5500	4
hsa05205	Proteoglycans in cancer	0.002127	7448/5499/5501/5500	4
hsa04024	cAMP signaling pathway	0.002584	5908/5499/5501/5500	4
hsa05031	Amphetamine addiction	0.000852	5499/5501/5500	3
hsa04750	Inflammatory mediator regulation of TRP channels	0.002594	5499/5501/5500	3
hsa04931	Insulin resistance	0.003228	5499/5501/5500	3
hsa04728	Dopaminergic synapse	0.005552	5499/5501/5500	3
hsa04270	Vascular smooth muscle contraction	0.005671	5499/5501/5500	3
hsa04910	Insulin signaling pathway	0.006288	5499/5501/5500	3
hsa04261	Adrenergic signaling in cardiomyocytes	0.007357	5499/5501/5500	3
hsa04921	Oxytocin signaling pathway	0.008528	5499/5501/5500	3
hsa04022	cGMP-PKG signaling pathway	0.010655	5499/5501/5500	3
hsa05034	Alcoholism	0.013263	5499/5501/5500	3
hsa04810	Regulation of actin cytoskeleton	0.021015	5499/5501/5500	3
hsa04151	PI3K-Akt signaling pathway	0.074335	7448/7529/7534	3
hsa05168	Herpes simplex virus 1 infection	0.156307	5499/5501/5500	3
hsa05143	African trypanosomiasis	0.004709	335/3039	2
hsa04979	Cholesterol metabolism	0.008474	335/6646	2
hsa05230	Central carbon metabolism in cancer	0.014028	6510/3939	2
hsa00010	Glycolysis/Gluconeogenesis	0.015285	226/3939	2
hsa04066	HIF-1 signaling pathway	0.031472	226/3939	2
hsa04110	Cell cycle	0.046573	7529/7534	2
hsa05160	Hepatitis C	0.069208	7529/7534	2
hsa05161	Hepatitis B	0.075547	7529/7534	2
hsa04530	Tight junction	0.081244	4622/10207	2
hsa05203	Viral carcinogenesis	0.107976	7529/7534	2
hsa05165	Human papillomavirus infection	0.23603	7448/10207	2
hsa00100	Steroid biosynthesis	0.052004	6646	1
hsa04977	Vitamin digestion and absorption	0.065254	335	1
hsa00030	Pentose phosphate pathway	0.080921	226	1
hsa00640	Propanoate metabolism	0.086087	3939	1
hsa00051	Fructose and mannose metabolism	0.08866	226	1
hsa00620	Pyruvate metabolism	0.103952	3939	1
hsa04975	Fat digestion and absorption	0.108994	335	1
hsa00270	Cysteine and methionine metabolism	0.12396	3939	1
hsa05144	Malaria	0.128896	3039	1
hsa05130	Pathogenic *Escherichia coli* infection	0.143542	7534	1
hsa05134	Legionellosis	0.143542	81876	1
hsa00590	Arachidonic acid metabolism	0.162706	4048	1
hsa04137	Mitophagy - animal	0.167432	8878	1
hsa05211	Renal cell carcinoma	0.176809	5908	1
hsa03320	PPAR signaling pathway	0.188388	335	1
hsa01230	Biosynthesis of amino acids	0.190685	226	1
hsa04610	Complement and coagulation cascades	0.199812	7448	1
hsa04512	ECM-receptor interaction	0.206592	7448	1
hsa04146	Peroxisome	0.20884	25824	1
hsa04974	Protein digestion and absorption	0.224406	6510	1

Table 2. continued

ID	Description	*P* value	Gene ID	Count
hsa04972	Pancreatic secretion	0.241838	5908	1
hsa04922	Glucagon signaling pathway	0.252542	3939	1
hsa04670	Leukocyte transendothelial migration	0.271447	5908	1
hsa01200	Carbon metabolism	0.279702	226	1
hsa04722	Neurotrophin signaling pathway	0.285834	5908	1
hsa04380	Osteoclast differentiation	0.303934	8878	1
hsa05418	Fluid shear stress and atherosclerosis	0.325462	8878	1
hsa03010	Ribosome	0.351943	6223	1
hsa04934	Cushing syndrome	0.355644	5908	1
hsa04217	Necroptosis	0.36844	8878	1
hsa05164	Influenza A	0.37743	10898	1
hsa04360	Axon guidance	0.401959	23654	1
hsa04062	Chemokine signaling pathway	0.417237	5908	1
hsa04015	Rap1 signaling pathway	0.443483	5908	1
hsa04014	Ras signaling pathway	0.483741	5908	1
hsa04010	MAPK signaling pathway	0.570085	5908	1

B4 exhibited excellent antiviral efficacy in EV71-infected suckling mice

As B4 showed superior antiviral efficacy in vitro, to determine the efficacy of B4 in vivo, we used an EV71-infected suckling mice model for investigation (Fig. 6a). In this model, without drug administration, EV71 infection-related symptoms appeared on day 5 post infection and this was characterized mostly by weakness in the hind limbs. In later days, the condition of EV71-infected mice further deteriorated into hind limb or front limb paralysis and reached a peak at day 6–10 post-infection (Fig. 6b). On the other hand, B4 administration significantly alleviated these symptoms, as observed clinical scores were markedly lower than that in the EV71 group (Fig. 6b, $P < 0.01$ Wilcoxon rank test). As for the mortality of challenged mice, the group of B4 injection at 200 mg·kg^{-1} was almost completely protected (95.0% survival, Fig. 6c) whereas the EV71 group yielded a 55.6% survival at the end of the observation ($P < 0.01$, Mantel–Cox test). Histological observation revealed massive myofibril fracture and myocyte disruption, necrotizing myositis with inflammatory infiltrates in the limb muscles, and intercostal spaces even along the spine in the EV71 group (Fig. 6d, see black arrows). B4 administration significantly improved the integrity of limb muscle structure, although slight damages were still observed (Fig. 6d, see black asterisks). Furthermore, systemic inflammatory response syndrome caused by virus infection is a typical consequence that may result in sepsis. It was reported that EV71-infected mice exhibited a subtle and transient elevation in IL-10 and IFN-γ, which was associated with the pathogenesis of HMFD [27]. Interestingly, the anti-inflammatory cytokine IL-10 was significantly increased (Fig. 6e), with the decline of IFN-γ (Fig. 6f) in the B4-treated mice.

At last, in order to confirm the activation of type I IFN response in B4-treated mice, the expression of IFN-β was detected in EV71-infected suckling mice model. The qRT-PCR results showed a significant increase in IFN-β mRNA (Fig. 6h) and dramatic decline in viral RNA when B4 was administered (Fig. 6g). Immunohistochemistry staining of VP-1 and IFN-β was employed to evaluate the extent of viral inhibition and type I IFN induction caused by B4. Skeletal muscle tissues exhibited positive staining, as intensive and widespread signal was detected, indicating IFN-β expression (Fig. 6i, see black asterisks) in the B4-treated group. Meanwhile, VP-1 expression was largely suppressed by B4 in the muscle (Fig. 6i, see black arrows). These results revealed that B4 exhibited excellent antiviral efficacy and type I IFN induction efficacy in vivo.

DISCUSSION

There is currently no effective antiviral drug available to treat patients infected by EV71. Although the EV71 vaccine protected EV71-associated HFMD [28], another important question that viral RNA gives rise to frequent mutations in the newly synthesized viral genome, possibly restricting the use of vaccines [29]. Therefore, searching for effective antiviral drugs that target the host immune response is an advisable strategy. According to the theory of traditional Chinese medicine, HFMD is mainly caused by an accumulation of *damp-heat* and *toxicity* in the body [30], and its treatment may involve the usage of *heat-clearing* and *detoxifying* medicines [31]. Accordingly, many medicinal plant extracts and natural products with *heat-clearing* and *detoxifying* activities are worthy to be investigated. In addition to direct antiviral potencies, some medicinal plant extracts and natural products also exert anti-inflammatory effects to suppress the excessive inflammatory response caused by viral infection or regulate the immune system to resist viral infection. *P. chinensis* is a medicinal plant with a long history of use for *heat-clearing* and *detoxification*, used for the treatment of intestinal diseases, such as amebic dysentery [32]. A previous study showed B4, the major saponin component of *P. chinensis*, exhibited anti-inflammatory and immune-modulatory activities [21]. Here, we evaluated the antiviral activities of B4 against EV71 in cell cultures. B4 was a potential antiviral agent, with an IC_{50} value of 24.95 ± 0.05 μM on the EV71 replication in RD cells. Moreover, B4 could also effectively inhibit viral titer and viral protein in a dose-dependent manner.

It has been accepted that host immune responses resulting from virus infection play a vital role in clearing the infection. Activating or restoring the IFN system in an organism is critical for the initiation of host immune responses [12, 33]. Therefore, an IFN-inducing agent, which could also stimulate the response of type I IFNs, should be a high-priority target for antiviral drug development. In this study, we measured the expression of IFN-β and the downstream antiviral effectors IFN-stimulated genes, such as MxA, upon B4 administration. As reported in the previous study [34], the host cells could sense EV71 infection and stimulate IFN-β production. However, the levels of downstream IFN-stimulated

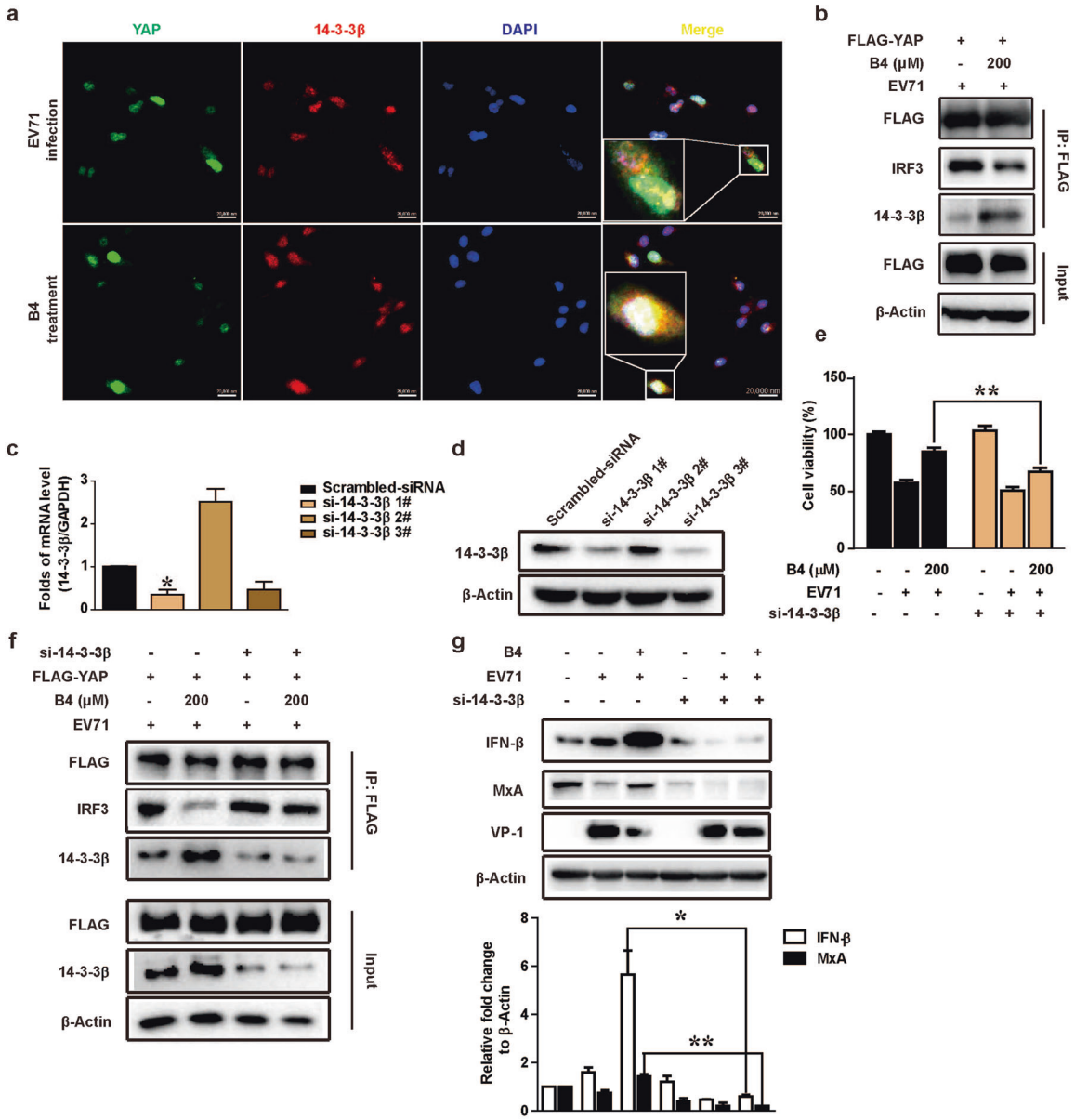

Fig. 5 B4 increased the interaction with 14-3-3β and YAP and 14-3-3β is critical for the antiviral activity of B4. a Representative confocal microscope image showing co-localization of YAP and 14-3-3β in EV71-infected cell with or without B4 administration. RD cells were immune-stained with antibodies against 14-3-3β (red) and YAP (green), Scale bar = 20 μm; **b** Immunoprecipitation with anti-FLAG. Western blot analysis of the interaction between YAP and 14-3-3β or IRF3. HEK293T cells were transfected with Flag-YAP plasmids for 24 h and then infected with EV71 after B4 treatment. IP was performed with anti-Flag M2 affinity gel, then protein interaction was detected by immunoblot; Input, the whole-cell lysates without immunoprecipitated; **c** RD cells were transfected with si-14-3-3β or scrambled-siRNA for 48 h, and 14-3-3β mRNA levels were determined by qRT-PCR. GAPDH was also analyzed as internal control; **d** RD cells were transfected with si-14-3-3β or scrambled-siRNA for 48 h, and 14-3-3β levels were evaluated by immunoblotting with 14-3-3β antibodies. β-Actin was also analyzed as loading control; RD cells were transfected with 14-3-3β specific siRNA and control siRNA for 24 h and then infected with EV71 after B4 treatment. **e** Antiviral activity was determined by the cell viability assay. Cell viability of transfected scrambled-siRNA cells was set 100%; **f** Immunoprecipitation with anti-FLAG. Western blot analysis of the interaction between YAP and 14-3-3β or IRF3; **g** The levels of IFN-β, MxA, and VP-1 were evaluated by immunoblotting with IFN-β, MxA, and VP-1 antibodies. β-Actin was also analyzed as loading control. Data are presented as mean ± SD ($n = 3$). *$P < 0.05$, **$P < 0.01$.

gene MxA could not be successfully induced and even suppressed by EV71. Interestingly, we found that B4 could enhance the induction of IFN-β and robust the IFN-β response in the EV71-infected cells. IRF3 is a well-characterized signaling mediator/transcription factor that is essential for RLRs pathway activation. Activated IRF3 dimerizes and enters the nucleus to regulate both type I IFN and IFN-stimulated genes [35]. Consistent with the results of previous studies [36], IRF3 activation was not observed in the cells that were infected with EV71. Moreover, p-IRF3 significantly decreased in 24 h of EV71 infection. However, B4 treatment could dramatically enhance the phosphorylation and translocation of IRF3. To the best of our knowledge, this is the first report on B4 as a potent inducer of IFN-β.

As IFN-β plays essential roles in innate immunity, we further examined the antiviral action of B4 upon IFN-β knockdown or deletion. We found that IFN-β knockdown suppressed the B4-induced improvement of EV71-infected cells viability and reduction of viral titer. Meanwhile, there was no difference in expression

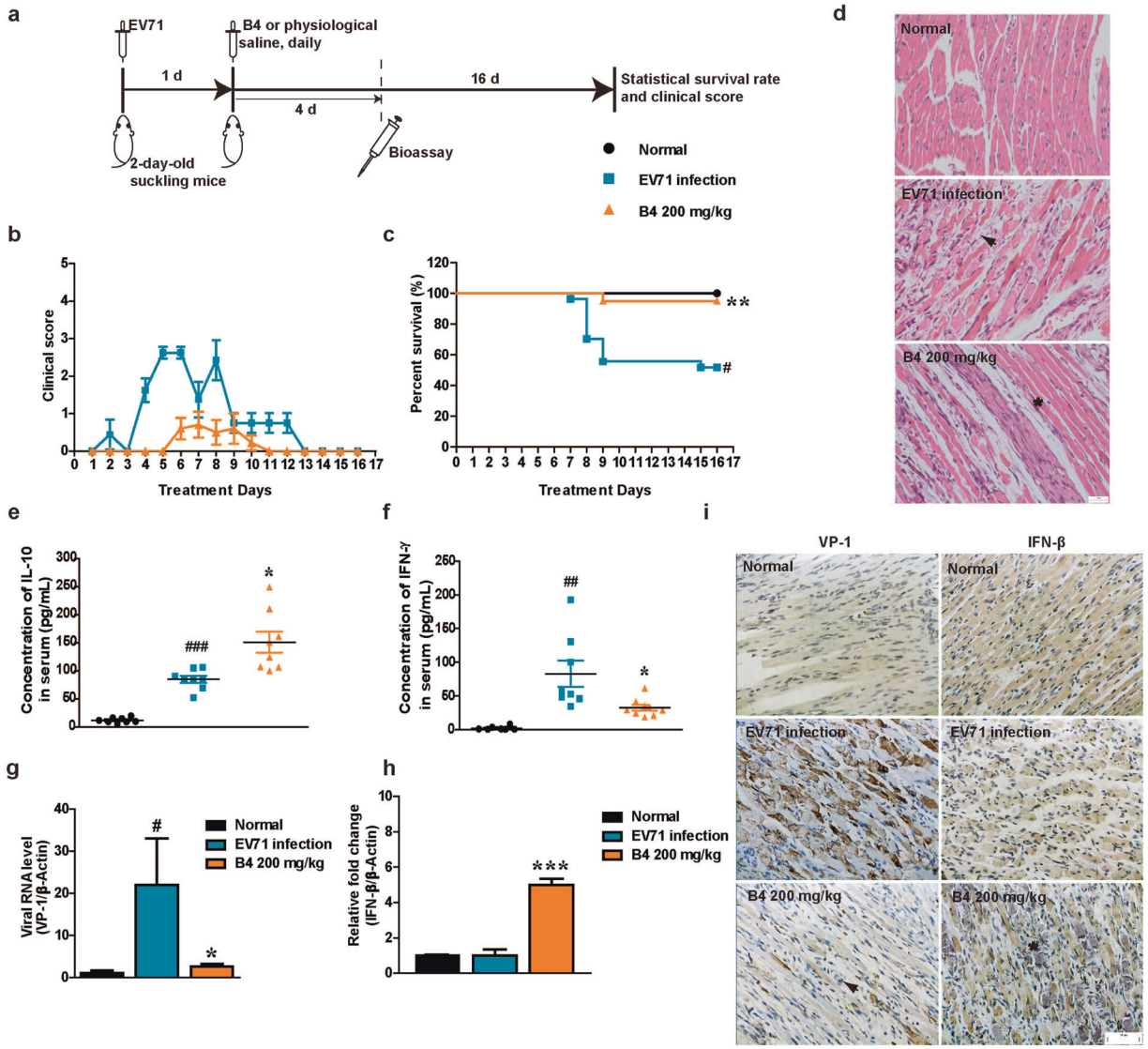

Fig. 6 B4 treatment improved survival and inhibited viral propagation in EV71-infected suckling mice model. a Schedule of EV71-infected suckling mice model; Clinical scores (**b**) and survival curve (**c**) of 2-day-old ICR mice i.p. inoculated with EV71 and treated with physiological saline ($n = 10$ mice), B4 (200 mg · kg^{-1}, $n = 10$ mice). Deaths were calculated into an average score only once at the first observed date; **d** Skeletal muscle samples were collected on day 5 post infection and subjected to H&E staining as described in the material and method section. Scale bar = 20 μm; the levels of IL-10 (**e**) and IFN-γ (**f**) in mouse serum were detected by MSD assay; total RNAs of skeletal muscle were prepared from different groups and subjected to qRT-PCR for the VP-1 region of EV71 viral RNA (**g**) and IFN-β (**h**). β-Actin was also analyzed as internal control; skeletal muscle samples were collected on day 5 post infection and subjected to immunohistochemistry (**i**) as described in the Materials and methods section. Scale bar = 20 μm. Data are presented as mean ± SD ($n = 10$). $^{\#}P < 0.05$, $^{\#\#}P < 0.01$, $^{\#\#\#}P < 0.001$ vs Normal control group; $^{*}P < 0.05$, $^{**}P < 0.01$, $^{***}P < 0.001$ vs physiological saline infection group.

of viral protein VP-1 and 3Cpro between IFN-β-knockdown cells and Scrambled-knockdown cells with B4 treatment. To confirm the essential role of IFN-β, we selected the Vero cell line to detect the antiviral efficacy of B4, because the gene loci encoding IFN-α/β are missing from the genomic DNA of Vero cells [37]. Indeed, B4 hardly exhibited antiviral efficacy in Vero cells. These results suggested that activation of host immune responses might be the antiviral mechanism of B4.

To gain more insight into the mechanisms behind the B4-regulated IFN-β induction, we analyzed the changes of infected cells' proteomes upon B4 treatment. SLIAC-based quantitative proteomics approach was used, 92 proteins were identified, and most of the proteins were found to be involved in critical biological processes, such as Hippo signaling pathway, focal adhesion, and mRNA surveillance pathway. Meanwhile, we found 6 proteins involved in the Hippo signaling pathway, that is PATJ (gene ID:10207), 14-3-3β (gene ID: 7529), 14-3-3ζ (gene ID: 7534), PPP1CA (gene ID: 5499), PPP1CB (gene ID: 5500), PPP1CC (gene ID: 5501). Interestingly, the previous study showed that 14-3-3 molecular scaffolds display widespread functions in diverse cellular processes including signal transduction, cell apoptosis, and type I IFN responses [38]. Previous studies showed that 14-3-3β functions as the regulatory switch of RIG-I-mediated inflammatory signal transduction [39], therefore, we focused on 14-3-3β for follow-up research, and confirmed the upregulated expression in the cytoplasm of B4-treated cells. Since 14-3-3 usually binds to phosphorylated serine/threonine (pS/T) residues, thereby influencing interactions of target proteins either by enabling or blocking the access to other proteins [40]. As reported 14-3-3 proteins could bind to YAP/TAZ transcriptional coactivators, preventing inhibition of IRF3 activation by cytoplasmic sequestration of YAP [13]. Our results inferred that B4 could significantly promote 14-3-

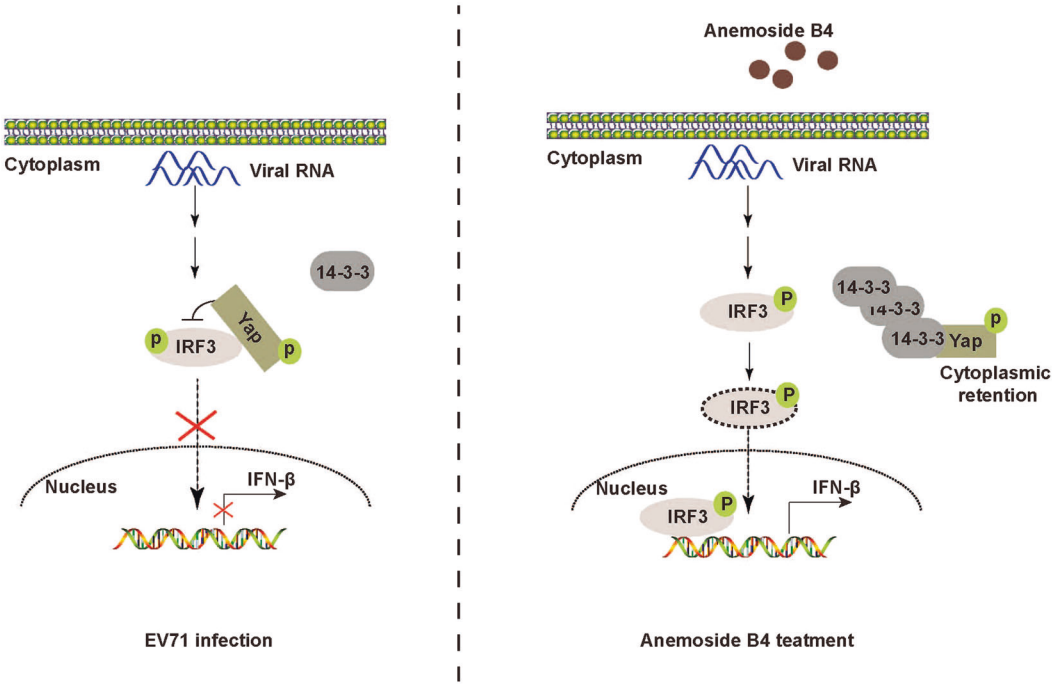

Fig. 7 Schematic diagram of the possible anti-EV71 mechanism of B4. Overview of B4 inhibits viral propagation through upregulating 14-3-3 and activating type I IFN response.

3β bind to YAP, and blocking the interaction of YAP and IRF3. Confocal immunofluorescence confirmed the colocalization of 14-3-3β and YAP in the cytoplasm of the infected cells after B4 treatment. In addition, the antiviral efficacy of B4 and innate immunity response were overall reduced in 14-3-3β-knockdown cells. We propose that 14-3-3β upregulation by B4 serves to cytoplasmic sequestration of YAP, and disrupt the downstream innate immune signaling retardation. Governance of 14-3-3 by B4 offers an effective approach for control of the innate immune response in infected cells. In addition, other studies showed that 14-3-3ζ interacted with and inhibited apoptotic effectors, such as Bad, caspase-2, and Bim, to promote cell survival [41]. These results could explain B4 slightly improved the survival of EV71-infected Vero cells and IFN-β/14-3-3β-knockdown cells.

Moreover, we employed the suckling mouse model [42] to evaluate the anti-EV71 effect of B4 in vivo. Encouragingly, the administration of B4 could strongly suppress EV71 replication and result in the improvement of muscle inflammation and limb activity. Meanwhile, B4 could also inhibit the expressions of HFMD biomarkers IL-10 and IFN-γ [43], attenuating complications of EV71 infection. To this end, activation of innate immunity pathway was confirmed by the expression of IFN-β in B4-treated mice.

CONCLUSION

Together with our current observations, these studies implicate B4, as a natural type I IFN signaling enhancer, can strongly inhibit EV71 propagation. By upregulating 14-3-3, B4 can enhance 14-3-3 interaction with YAP and activate type I IFN response (Fig. 7). Considering the low-toxic characteristics, B4 may serve as a potential lead compound for anti-EV71 drug development. Possible applications of B4 for other viral infections are presently being explored.

ACKNOWLEDGEMENTS

This work was jointly supported by the National Natural Science Foundation of China (Nos. 81903896, 82073912, 81273402), China Postdoctoral Science Foundation (No. 2021M692359), the Open Project of State Key Laboratory of Bioactive Substance and Function of Natural Medicines of Chinese Academy of Medical Sciences and Peking Union Medical College (No. GTZK202007), Suzhou Science and Technology Plan Project (SYS2019032), and Priority Academic Program Development (PAPD) of Jiangsu Higher Education Institutions.

AUTHOR CONTRIBUTIONS

QMX and NXK designed research. NXK, YZ, QHL, and YEW performed research. HDF established the animal model and performed the in vivo experiments. GQX contributed SLICA experiments and analytic tools. NXK analyzed the data and wrote the paper. DY, YLL, SLY, and QMX revised the paper. All authors read and approved the final paper.

ADDITIONAL INFORMATION

Supplementary information The online version contains supplementary material available at https://doi.org/10.1038/s41401-021-00733-1.

Competing interests: The authors declare no competing interests.

REFERENCES

1. Solomon T, Lewthwaite P, Perera D, Cardosa MJ, McMinn P, Ooi MH. Virology, epidemiology, pathogenesis, and control of enterovirus 71. Lancet Infect Dis. 2010;10:778–90.
2. McMinn PC. An overview of the evolution of enterovirus 71 and its clinical and public health significance. FEMS Microbiol Rev. 2002;26:91–107.
3. Zhuang ZC, Kou ZQ, Bai YJ, Cong X, Wang LH, Li C, et al. Epidemiological research on hand, foot, and mouth disease in mainland China. Viruses. 2015;7:6400–11.
4. Shih C, Liao CC, Chang YS, Wu SY, Chang CS, Liou AT. Immunocompetent and immunodeficient mouse models for enterovirus 71 pathogenesis and therapy. Viruses. 2018;10:674.
5. Mao QY, Wang Y, Bian L, Xu M, Liang Z. EV71 vaccine, a new tool to control outbreaks of hand, foot and mouth disease (HFMD). Expert Rev Vaccines. 2016;15:599–606.
6. Seth RB, Sun L, Ea CK, Chen ZJ. Identification and characterization of MAVS, a mitochondrial antiviral signaling protein that activates NF-κB and IRF 3. Cell. 2005;122:669–82.
7. Xu LG, Wang YY, Han KJ, Li LY, Zhai Z, Shu HB. VISA is an adapter protein required for virus-triggered IFN-β signaling. Mol Cell. 2005;19:727–40.

8. Kawai T, Takahashi K, Sato S, Coban C, Kumar H, Kato H, et al. IPS-1, an adaptor triggering RIG-I- and Mda5-mediated type I interferon induction. Nat Immunol. 2005;6:981–8.
9. Meylan E, Curran J, Hofmann K, Moradpour D, Binder M, Bartenschlager R, et al. Cardif is an adaptor protein in the RIG-I antiviral pathway and is targeted by hepatitis C virus. Nature. 2005;437:1167–72.
10. Chan YK, Gack MU. RIG-I-like receptor regulation in virus infection and immunity. Curr Opin Virol. 2015;12:7–14.
11. Wang B, Xi XY, Lei XB, Zhang XY, Cui S, Wang JW, et al. Enterovirus 71 protease 2Apro targets MAVS to inhibit anti-viral type I interferon responses. PLoS Pathog. 2013;9:e1003231.
12. Pathinayake PS, Hsu AC, Wark PA. Innate immunity and immune evasion by enterovirus 71. Viruses. 2015;7:6613–30.
13. Munoz-Wolf N, Lavelle EC. Hippo interferes with antiviral defences. Nat Cell Biol. 2017;19:267–9.
14. Zhang Q, Meng F, Chen S, Plouffe SW, Wu S, Liu S, et al. Hippo signalling governs cytosolic nucleic acid sensing through YAP/TAZ-mediated TBK1 blockade. Nat Cell Biol. 2017;19:362–74.
15. Wang LY, Wang JF, Wang LS, Ma SR, Liu YH. Anti-enterovirus 71 agents of natural products. Molecules. 2015;20:16320–33.
16. Liu Q, Chen WC, Jiao Y, Hou JQ, Wu QY, Liu YL, et al. *Pulsatilla saponin* A, an active molecule from *Pulsatilla chinensis*, induces cancer cell death and inhibits tumor growth in mouse xenograft models. J Surg Res. 2014;188:387–95.
17. Liu T, Ye LG, Guan XQ, Liang XS, Li C, Sun Q, et al. Immunopontentiating and antitumor activities of a polysaccharide from *Pulsatilla chinensis* (Bunge) Regel. Int J Biol Macromol. 2013;54:225–9.
18. Sun YX, Liu JC, Yu HT, Gong CJ. Isolation and evaluation of immunological adjuvant activities of saponins from the roots of *Pulsatilla chinensis* with less adverse reactions. Int Immunopharmacol. 2010;10:584–90.
19. Hu YY, He KW, Wang XM. Role of Chinese herbal medicinal ingredients in secretion of cytokines by PCV2-induced endothelial cells. J Immunotoxicol. 2016;13:141–7.
20. Hu YY, Chen X, Duan HQ, Hu YL, Mu X. Pulsatilla decoction and its active ingredients inhibit secretion of NO, ET-1, TNF-alpha, and IL-1 alpha in LPS-induced rat intestinal microvascular endothelial cells. Cell Biochem Funct. 2009;27:284–8.
21. Kang NX, Shen WH, Zhang Y, Su ZT, Yang SL, Liu YL, et al. Anti-inflammatory and immune-modulatory properties of anemoside B4 isolated from *Pulsatilla chinensis* in vivo. Phytomedicine. 2019;64:152934.
22. Zhang XN, Song ZG, Qin BY, Zhang XL, Chen LX, Hu YW, et al. Rupintrivir is a promising candidate for treating severe cases of enterovirus-71 infection: evaluation of antiviral efficacy in a murine infection model. Antivir Res. 2013;97:264–9.
23. Xu TH, Xu YJ, Li HX, Han D, Zhao HF, Xie SX, et al. Two new triterpenoid saponins from Pulsatilla cernua (Thunb.) Bercht. et Opiz. J Asian Nat Prod Res. 2007;9:705–11.
24. Lu FQ, Sun XH, Xu XF, Jiang XG. SILAC-based proteomic profiling of the suppression of TGF-β1-induced lung fibroblast-to-myofibroblast differentiation by trehalose. Toxicol Appl Pharmacol. 2020;391:114916.
25. Dragan AI, Hargreaves VV, Makeyeva EN, Privalov PL. Mechanisms of activation of interferon regulator factor 3: the role of C-terminal domain phosphorylation in IRF-3 dimerization and DNA binding. Nucleic Acids Res. 2007;35:3525–34.
26. Prescott J, Hall P, Acuna-Retamar M, Ye C, Wathelet MG, Ebihara H, et al. New World hantaviruses activate IFNlambda production in type I IFN-deficient vero E6 cells. PLoS One. 2010;5:e11159.
27. Huang SW, Lee YP, Hung YT, Lin CH, Chuang JI, Lei HY, et al. Exogenous interleukin-6, interleukin-13, and interferon-γ provoke pulmonary abnormality with mild edema in enterovirus 71-infected mice. Respir Res. 2011;12:147.
28. Zhu FC, Xu WB, Xia JL, Liang ZL, Liu Y, Zhang XF, et al. Efficacy, safety, and immunogenicity of an enterovirus 71 vaccine in China. N Engl J Med. 2014;370:818–28.
29. Kuo RL, Shih SR. Strategies to develop antivirals against enterovirus 71. Virol J. 2013;10:28.
30. Li T, Peng T. Traditional Chinese herbal medicine as a source of molecules with antiviral activity. Antivir Res. 2013;97:1–9.
31. Wang MJ, Tao L, Xu HX. Chinese herbal medicines as a source of molecules with anti-enterovirus 71 activity. Chin Med. 2016;11:2.
32. Suh SY, An WG. Systems pharmacological approach of Pulsatillae radix on treating Crohn's disease. Evid Based Complement Altern Med. 2017;2017:4198035.
33. Iwasaki A, Pillai PS. Innate immunity to influenza virus infection. Nat Rev Immunol. 2014;14:315–28.
34. Lu J, Yi L, Zhao J, Yu J, Chen Y, Lin MC, et al. Enterovirus 71 disrupts interferon signaling by reducing the level of interferon receptor 1. J Virol. 2012;86:3767–76.
35. Jiao S, Guan JM, Chen M, Wang WJ, Li CC, Wang YG, et al. Targeting IRF3 as a YAP agonist therapy against gastric cancer. J Exp Med. 2018;215:699–718.
36. Chen N, Li XZ, Li PF, Pan ZY, Ding Y, Zou DH, et al. Enterovirus 71 inhibits cellular type I interferon signaling by inhibiting host RIG-I ubiquitination. Micro Pathog. 2016;100:84–89.
37. Emeny JM, Morgan MJ. Regulation of the interferon system: evidence that Vero cells have a genetic defect in interferon production. J Gen Virol. 1979;43:247–52.
38. Gupta S, Yla-Anttila P, Sandalova T, Sun R, Achour A, Masucci MG. 14-3-3 scaffold proteins mediate the inactivation of trim25 and inhibition of the type I interferon response by herpesvirus deconjugases. PLoS Pathog. 2019;15:e1008146.
39. Yang CS, Rodgers M, Min CK, Lee JS, Kingeter L, Lee JY, et al. The autophagy regulator Rubicon is a feedback inhibitor of CARD9-mediated host innate immunity. Cell Host Microbe. 2012;11:277–89.
40. Aghazadeh Y, Papadopoulos V. The role of the 14-3-3 protein family in health, disease, and drug development. Drug Discov Today. 2016;21:278–87.
41. Matta A, Siu KW, Ralhan R. 14-3-3 zeta as novel molecular target for cancer therapy. Expert Opin Ther Targets. 2012;16:515–23.
42. Chumakov M, Voroshilova M, Shindarov L, Lavrova I, Gracheva L, Koroleva G, et al. Enterovirus 71 isolated from cases of epidemic poliomyelitis-like disease in Bulgaria. Arch Virol. 1979;60:329–40.
43. Duan GC, Yang HY, Shi LB, Sun WM, Sui ML, Zhang RG, et al. Serum inflammatory cytokine levels correlate with hand-foot-mouth disease severity: a nested serial case-control study. PLoS One. 2014;9:e112676.